1

Introduction

1.1 Whispering-Gallery-Mode Microcavities

Optical resonant cavities, composed of two or more mirrors, are essential part of ordinary lasers and have been utilized in almost all branches of modern optics and photonics. Optical energy is recirculated inside the cavities due to the reflection on the mirrors, and one basic property of the optical cavities is the quality (Q) factor related to the mode lifetime for describing the light-confining ability. Mode volume (V) is another important parameter of an optical cavity and a small V is of great importance for realizing a compact-size integrated device. A suitable parameter, *finesse*, which is defined as the ratio of the free spectral range to the resonance linewidth, takes both the mode Q factor and the resonator size into account. For certain applications, high-finesse microcavity with a large value of Q/V, which is also related to the electromagnetic field enhancement factor of an optical cavity, is very important. Compared with conventional lasers, microcavity lasers with a large Q/V can promise lower lasing threshold. Moreover, light–matter interactions can be greatly enhanced by storing optical energy in a small mode volume [1, 2]. The ability to concentrate light is important to both fundamental science studies and practical device applications [3], such as strong-coupling cavity quantum electrodynamics, enhancement and suppression of spontaneous emission, high-sensitivity sensors, low-threshold light sources, and compact optical add-drop filters in optical communication.

To obtain high Q modes in optical cavities with a small V, a high reflectivity close to unity is necessary, which can be realized by utilizing a periodic structure to construct a photonic forbidden band, such as that in vertical-cavity surface-emitting lasers and photonic crystal microcavities, or simply by total internal reflection (TIR) at the dielectric boundary with a high-low refractive index contrast in whispering-gallery (WG)-mode optical microcavities [4]. The idea of WG mode was born out of the observation of acoustical phenomenon in [5] where sound waves were efficiently reflected with minimal diffraction and struck the wall again at the same angle and thereby traveled along the gallery surface. Similarly, classical electromagnetic waves can undergo reflection, refraction, and diffraction like the sound waves when the wavelengths of the waves are smaller than the bending radius of a reflection mirror. Among various kinds of optical microcavities, WG-mode microcavities with simple

Microcavity Semiconductor Lasers: Principles, Design, and Applications, First Edition.
Yong-zhen Huang and Yue-de Yang.

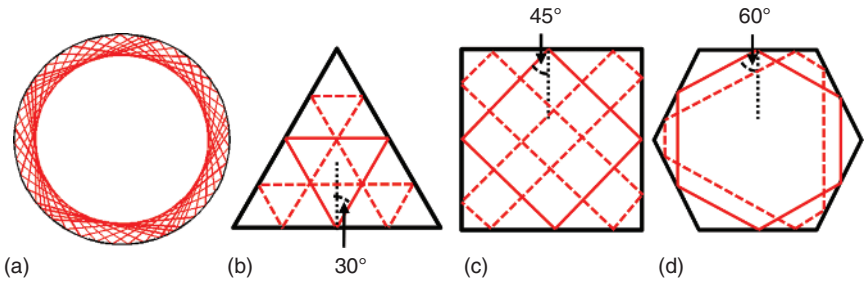

Figure 1.1 Schematic diagrams of (a) circular, (b) triangular, (c) square, and (d) hexagonal microcavities with the confined TIR light rays.

cavity geometries and suitability for planar integration play an important role in photonics integration nowadays [6–8]. WG-mode optical microcavities formed by various materials have been studied, such as liquid droplet, glass, crystal, polymer, and semiconductor [8].

The concept of WG mode was subsequently extended to the radiofrequency and optical domains for the electromagnetic waves. For WG-mode microcavities, the optical modes will experience ultra-low loss as the light rays are guided by continuous TIR at the boundaries. In fact, light guidance by continuous TIR is quite common in modern optics and photonics, such as the propagating optical modes in fibers and waveguides. The incident angles of the light rays in WG-mode microcavities are greater than the TIR criticality at all boundaries, and the light rays are mostly like to propagate along the WG surface. There are various kinds of WG-mode optical microcavities to maintain continuous TIR for the confined light rays. Figure 1.1 schematically shows circular, triangular, square, and hexagonal microcavities with the confined TIR light rays. As a natural choice, WG-mode optical microcavities with circular shapes, which maintain a perfect rotational symmetry, have attracted most research interest for the demonstration of low-power-consumption compact-size photonic devices, e.g. microdisk lasers [9]. In circular microcavities, the light ray confined inside the cavity has a conserved incident angle above the TIR critical angle resulting in ultrahigh Q factors and isotropic near- and far-field patterns. However, for a practical device, efficient input or output coupling is crucial but can be hardly achieved in the circular-shaped microcavities. By deforming the WG microcavity to a noncircular cavity shape, the far-field emission patterns can be modulated while high Q factor mode is maintained [10, 11].

1.2 Applications of Whispering-Gallery-Mode Microcavities

WG-mode optical microcavities with the light rays confined by continuous TIR at the cavity boundaries have unique mode properties, including high Q factors, small mode volume, and planar integration capability. Due to these mode properties, there has been a wide range of applications for WG-mode microcavities in

both fundamental physics and practical devices [12]. In this section, part of the applications, including photonic filters, sensors, and microlasers, based on both passive and active WG-mode microcavities, is briefly summarized.

One basic application of microcavities is photonic filter based on the wavelength selectivity property of WG modes, including all-pass and add-drop filters. A common microcavity-based filter includes a WG-mode microcavity and optical coupler for coupling light into or out from the WG modes [13–15]. In an optical filter, the filtering response is relative to both the intrinsic mode Q factors and the coupling coefficients for the WG modes. The high-order transverse WG modes have lower Q factors but stronger coupling, which is undesirable for most filtering applications. Hence, microrings are utilized for suppressing high-order transverse modes and realizing high-performance optical filter. Microrings have similar mode properties with the microdisks, as the modes are confined by the continuous TIR at the outer boundaries [14]. A typical on-chip all-optical four-port add-drop filter includes a microring cavity and two evanescent-field coupled waveguides. The add-drop filter exhibits pass-band filtering characteristics with the on-resonance light dropping through the drop port. The microring-based filters and corresponding active devices have the advantages of compact size, narrow band, and a large free spectral range, and have been widely studied in the silicon photonics for on-chip optical interconnection application. The pass-band characteristics can be further improved by using higher-order filter structure with multiple coupled microrings. Based on the microring photonic filters, cascaded microring-based matrix switches have been demonstrated for on-chip optical networks [16]. The networks-on-chip can be passive networks with fixed-wavelength assignment and switching networks with the resonance wavelength tuning by thermal effect or carrier injection. With the structure of all-pass microring filter, silicon-based microring electro-optic modulators were demonstrated with the carrier injection or depletion to change the resonance wavelength of the microring cavity [17].

Another important application of WG optical microcavities is photonic sensing. WG microcavities have been extensively investigated for their applications in chemicals and biosensing. Strong light–matter interactions and high optical energy intensity in the optical microcavities with a large value of Q/V can help to achieve ultrasensitive and label-free detection. The sensing principle is to measure the spectral changes of a WG mode in response to changes in the environment, e.g. refractive index shift of surrounding media or nanoparticles onto the cavity surface [18, 19]. The key feature is the strong evanescent field of the WG mode that propagates along and extends from the surface of the microcavity leading to strong interaction between the internal field and the external environment. The measured transmission spectra will experience a wavelength shift and/or splitting for sensing. The resonance shift in a microcavity is a more direct detection scheme, but it can be easily perturbed by environmental noises resulting in a reduction of the sensing resolution. The environmental noises are minimized in the mode splitting–based detection scheme as the two split modes suffer the same noises. The variation of mode splitting carries the information of particles to be measured. The detection resolution for a passive microcavity-based sensing is limited by the linewidth of

the WG modes. In a microcavity laser–based active sensing devices, the stimulated emission will narrow down the linewidth, and hence the sensing resolution is greatly enhanced [20]. For a cold cavity with a Q factor of 10^8, the laser linewidth can be as narrow as a few Hertz allowing ultrasensitive detection [8].

Light sources, such as microlasers and quantum sources, are an extremely important research direction in optics and photonics. Compared to other optical cavities for laser application, the WG-mode microcavities have extraordinarily high Q factor and small V, which lead to diverse applications in the study of laser physics and the realization of compact-size microlasers. In WG-mode microcavities, the optical density of states can be modulated by designing the cavity structure and matching the resonance wavelength to the emission wavelength of the active material. Thus, the Purcell factor can be enhanced greatly in optical microcavities [1]. Semiconductor quantum dot is a quasi-atom gain material; the coupling between the quantum dot and the optical mode can be enhanced in the high Q microcavity with a ultrasmall V. Strong coupling of a single GaAs quantum dot to a WG mode of a microdisk has been observed, facilitating the investigations of cavity quantum electrodynamics and single photon source [21]. High Q factor and small V also allow the demonstration of conventional low-threshold semiconductor microlasers [9]. The high Q factor of a WG mode guarantees a low-threshold current density and a small V leads to a compact size for the microlaser for achieving low-power consumption. Continuous wave lasing with a threshold of 40 μA was realized in an InGaAsP microdisk laser at room temperature [22]. However, the nearly perfect confinement of the mode light ray and the rotational symmetry of a circular microcavity led to low-output power and isotropic emission to free space despite a low-lasing threshold. This is a serious problem for most practical applications of WG microcavity lasers. Evanescent wave coupling of a waveguide is one traditional scheme to couple lasing light out from the circular microcavity lasers, but it has extremely high requirements for fabrication processing technology and parameter control. Experimental results show that a small variation in the coupling gap will reduce the output optical power by several orders of magnitude. In addition, the competition between the clockwise and counterclockwise modes in the circular microcavities will cause instability of the output optical power in the waveguide. To realize directional lasing emission, various deformed microcavities, such as adding local boundary defects or using smoothly deformed cavity shapes, have been proposed and demonstrated [3]. By carefully designing the cavity geometries, directional emission, or even unidirectional emission with low divergence angle in free space was achieved for deformed microcavity lasers while preserving high-Q WG modes for low-threshold lasing. However, the directional or unidirectional emission of asymmetric microcavities is still limited to free space, and the application to on-chip photonic integration requires waveguide-coupled output. Moreover, regular-polygonal-shaped microcavities have distinct mode properties, as the WG modes distribute nonuniformly along the cavity boundaries. A waveguide directly connecting to the position with weak mode field can be used for realizing a waveguide-coupled microcavity laser without strong perturbation to the corresponding high Q WG mode. Especially, a quasi-analytical solution can be obtained

for the equilateral-triangular and square microcavities with integrable internal dynamics, making them a reliable solution to demonstrate waveguide-coupled unidirectional-emission semiconductor microlasers [23].

1.3 Ultra-High *Q* Whispering-Gallery-Mode Microcavities

Spherical optical microcavities of liquid droplets and highly transparent silica have been extensively investigated, which can have nearly perfect microspheres due to surface tension of liquid and fused silica [1]. Based on liquid droplet microcavities, cavity quantum electrodynamics with modified spontaneous and stimulated emission spectra were studied and ultralow threshold of nonlinear optical processes was observed with fluorescent dyes. The effects of droplet deformation on the resonance frequencies and *Q* factors were investigated experimentally and theoretically using first-order perturbation theory, and the dye-lasing spectra from liquid droplet optical microcavities were observed under perturbations. By using the CO_2 laser fusion process, high-*Q* silica microspheres were fabricated by fusing the end of a silica fiber. WG modes with *Q* factors up to $10^9 \sim 10^{10}$ were observed, and low-threshold microlasers based on silica microspheres with doped irons were realized. Droplet microlasers as easily replaced coherent light sources were investigated for potential applications in integrated lab-on-a-chip systems [24]. The droplet-based microlasers can be prepared in microfluidic chip with different active media, such as live bacteria. In addition, intracellular droplet microlasers were studied by injecting oil doped with a dye gain medium inside biological cells as luminescent probes [25].

Ultra-high-*Q* microcavities can also be fabricated on a silicon wafer using wafer-scale processing, in the form of a microcavity on-a-chip suitable for photonic integrated circuits [2]. The fabrication processing is simply summarized in the following. First, silica circular patterns were transformed from photoresist layer to the thermally oxidized surface layer of a silicon wafer using lithography and etching technique processes, and then silica disks were used as an etching mask for selectively removing the underneath silicon. Finally, silica microdisks on a silicon post were fabricated with a vertical optical confined by air for avoiding a leaking loss into high-index silicon substrate. The WG modes with *Q*-factors up to 3×10^6 were measured for such microdisks under optimal processing conditions. As the mode-field distributions located near the disk periphery, the *Q*-factors were mainly limited by scattering loss due to disk roughness caused by lithography and etching. To further increase mode *Q* factors, a reflow process for the silica microdisks was applied under the surface-normal irradiation of CO_2 laser by improving surface smooth of the microdisks without affecting the underneath silicon post. The reflow process under the laser irradiation can lead to melting and collapse of the silica at the disk periphery and form silica microtoroid on a silicon chip. The ultra-high *Q* factor based on linewidth measurement is a challenge as a loaded cavity *Q* factor is measured with coupled waveguide. In addition, WG mode splits into doublets caused by weak back scattering in the microcavity, and

thermal effects due to input optical power induce distortion of the resonance peak. An intrinsic cavity Q factor of 4.3×10^8 was obtained by cavity ring-down measurement for a microtoroid cavity mode. The WG mode loss is negligible for microtoroids with principal tori-radii larger than 15 μm, and measured Q values are more than 10^8 in the wavelength of 1550-nm band. The ultra-high-Q microcavities are especially suitable to study optical nonlinear processes, such as Raman and Kerr nonlinearities. Under fiber evanescently coupling with a low-input power at resonant frequency, high-mode field intensity can be stored inside an ultra-high-Q microcavity for ultra-low-threshold fiber-compatible Raman lasers and parameter oscillators. Furthermore, optical frequency combs were realized through cascaded four-wave mixing process in a high Q microresonator [26].

In addition, chemically etched wedge resonators on-a-chip were fabricated using conventional semiconductor processing, with a Q factor of 875 million surpassing microtoroids [27]. The smoothness of wedge resonators was improved using post exposure bake method to cure the roughness of photoresist patterns and extend the chemically etched time to form wedge profiles for the resonator perimeter. Without the reflow process of laser irradiation, the wedge resonators are of easy-to-control size and can be integrated with other photonic devices.

1.4 Mode *Q* Factors for Semiconductor Microlasers

1.4.1 Output Efficiency and Mode *Q* Factor

For a microcavity laser, as shown in Figure 1.2, with a passive cavity mode Q factor Q_R related to planar and vertical radiation losses α_r and α_v and an output coupling loss α_o, we can have a modified mode lifetime varied with a mode gain Γg as:

$$\tau_p = \frac{1}{v_g \alpha_i + \omega/Q_R - \Gamma v_g g}, \tag{1.1}$$

where Γ is the optical confinement factor, α_i is an internal material absorption loss, $v_g = c/n_g$ is the light group speed with a group index n_g, and ω is the mode angular frequency. Mode Q_T factor, including the absorption loss, can be defined as:

$$\frac{1}{Q_T} = \frac{1}{Q_R} + \frac{\alpha_i v_g}{\omega} = \frac{1}{Q_R} + \frac{1}{Q_A}. \tag{1.2}$$

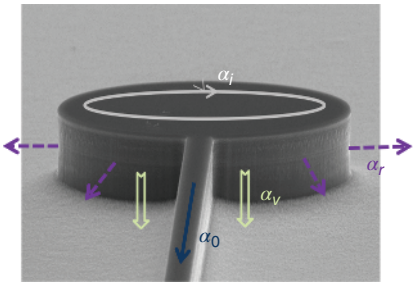

Figure 1.2 Scanned electron micrograph image of a microdisk connected with an output waveguide.

For a silica microdisk without gain and $\alpha_i \approx 0$, it is easy to measure mode Q factor from the transmission linewidth because $Q_T = Q_R$. However, semiconductor lasers usually have an absorption loss, which limited mode Q factors. Taking the absorption loss $\alpha_i = 1$ and $10\,\mathrm{cm}^{-1}$, which corresponds to the magnitude of the absorption loss for GaAs and InP system semiconductor lasers, respectively, we have mode Q_A factor of 1.4×10^5 and 1.4×10^4 at $n_g = 3.5$ and mode wavelength of 1550 nm.

Accounting for the internal absorption loss α_i related to Q_A, output coupling loss through the output waveguide α_o, the vertical loss α_v into the substrate, and the other radiation loss, including scattering loss due to rough perimeter α_r, we can define an output efficiency as

$$\eta = \frac{\alpha_o}{\alpha_i + \alpha_o + \alpha_r + \alpha_v} = \frac{\alpha_o}{\alpha_o + \alpha_v + \alpha_r}\frac{Q_T}{Q_R} = \frac{\alpha_o}{\alpha_o + \alpha_v + \alpha_r}\frac{Q_A}{Q_A + Q_R}. \tag{1.3}$$

The laser output efficiency will be very low for an ultra-high Q microcavity with $Q_R \gg Q_A$. The material of low absorption loss with a high Q_A is important for realizing high-output efficiency for a microlaser.

1.4.2 Measurement of Mode *Q* Factor

The mode Q factors of a microlaser are usually measured as the ratio of mode wavelength to the full-width at half maximum (FWHM) of the resonator peak at the threshold. The mode linewidth is described by the Schawlow–Townes linewidth formula below the threshold [28]:

$$\Delta\lambda = \frac{\lambda^2}{2\pi c\tau_p} = \frac{\lambda^2 \Gamma \beta B n^2}{2\pi c s}. \tag{1.4}$$

Due to the gain-refractive index coupling effect with a linewidth enhancement factor α and carrier density clamping above threshold, lasing mode linewidth above the threshold is given by the modified Schawlow–Townes linewidth formula [29]:

$$\Delta\lambda = \frac{\lambda^2(1+\alpha^2)}{4\pi c\tau_p}, \tag{1.5}$$

which is equal to (1.4) multiplying by a factor of $(1+\alpha^2)/2$. The laser linewidth enhancement near threshold was observed experimentally for semiconductor microlasers [30].

The output characteristics of semiconductor microcavity lasers can be described by the following single-mode rate equations

$$\frac{dn}{dt} = \frac{\eta_i I}{qV_a} - An - Bn^2 - Cn^3 - v_g g(n)s, \tag{1.6}$$

$$\frac{ds}{dt} = v_g[\Gamma g(n) - \alpha_i]s - \frac{s}{\tau_{pc}} + \Gamma\beta B n^2, \tag{1.7}$$

where s is the photon density, n is the carrier density, I is the injection current, η_i is the injection efficiency, q is the electron charge, V_a is the volume of the active region, A, B, and C are the defect, bimolecular, and Auger recombination coefficients, respectively, β is the spontaneous emission factor, and $\tau_{\mathrm{pc}} = Q_R/\omega$ is the

passive cavity mode lifetime. The threshold gain of semiconductor lasers is usually expressed as

$$\Gamma g = \alpha_i + \frac{\omega}{Q_R v_g}, \tag{1.8}$$

which is only approached in the steady state. From Eq. (1.7), we can obtain the output term in steady state as

$$\frac{s}{\tau_{pc}} = v_g[\Gamma g(n) - \alpha_i]s + \Gamma \beta B n^2. \tag{1.9}$$

The mode lifetime is determined by the passive cavity Q_R factor as $\Gamma g = \alpha_i$ from (1.1), so the passive mode Q_R factor should be measured at the following condition

$$\Gamma g = \alpha_i, \tag{1.10}$$

instead of threshold gain of (1.8). However, it is difficult to determine the condition of (1.10) from the curve of the output power vs. injection current.

In the following part of this section, we give numerical results of the rate Eqs. (1.6) and (1.7). The gain coefficient is assumed to be a logarithmic function as [31]

$$g(n) = g_0 \ln\left(\frac{n + N_s}{N_{tr} + N_s}\right), \tag{1.11}$$

where g_0 is the material gain parameter, N_{tr} is the transparency carrier density, and N_s is a gain parameter. Taking the parameters as $\lambda = 1550$ nm, $N_{tr} = 1.2 \times 10^{18}$ cm^{-3}, $N_s = 1.1 \times 10^{18}$ cm^{-3}, mode group index $n_g = 3.5$, $\eta_i = 0.8$, $\Gamma = 0.1$, $A = 1 \times 10^8$ s^{-1}, $B = 1 \times 10^{-10}$ cm^{-3} s^{-1}, $C = 1 \times 10^{-28}$ cm^6 s^{-1}, $g_0 = 1500$ cm^{-1}, we numerically calculate the steady solutions of Eqs. (1.6) and (1.7), and plot the output powers and linewidths of Eqs. (1.4) and (1.5) vs. the injection current in Figure 1.3 at $Q_R = 60\,000$, 20 000, and 6000, and $\alpha_i = 4$ cm^{-1}, for microdisk lasers with a circular radius of

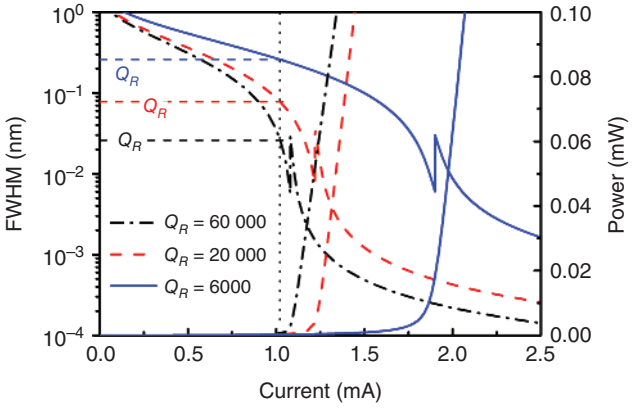

Figure 1.3 Laser-mode linewidth and output power vs. injection current for semiconductor microdisk lasers with $\beta = 10^{-3}$ at $Q_R = 60\,000$, 20 000, and 6000, and $\alpha_i = 4$ cm^{-1}. The three horizontal dashed lines correspond to the FWHMs determined by the Q_R factors, and vertical dotted line is at the condition of $\Gamma g = \alpha_i$.

10 μm, $\beta = 10^{-3}$, and a linewidth enhancement factor $\alpha = 3$. The output power is related to the mode photon density as

$$P = \frac{h\nu V_a s}{\Gamma \tau_{pc}}, \tag{1.12}$$

where $h\nu$ is the photon energy. The FWHMs determined by the Q_R factors are marked by the horizontal dashed lines. The FWHMs vary rapidly around the threshold, and Q factor measured using the FWHM at the threshold will overestimate the passive mode Q_R factor greatly.

The FWHMs at the vertical dashed line in Figure 1.3 should be used to calculate Q_R factors, which is difficult to determine from measured curve of output power vs. injection current. If the lasing mode output power can be divided into the first term and the second term of the right side of Eq. (1.9) from lasing spectra, we can calculate the derivative of the first term with respect to the output power and determine the condition of $\Gamma g = \alpha_i$ by finding the zero of the derivative.

Finally, we present experimental results for a microdisk laser as shown in Figure 1.1, with a radius of 8 μm and a 2-μm-wide output waveguide. The output powers vs. injection currents at 288, 290, and 296 K are presented in Figure 1.4a with magnified curves around threshold current in Figure 1.4b, where extrapolated lines are plotted as dashed lines. The practical output powers are limited by heating effect; even a thermoelectric cooler was used to control the temperature. The lasing spectra at 288 K and 10 mA are plotted in Figure 1.4c with single-mode operation

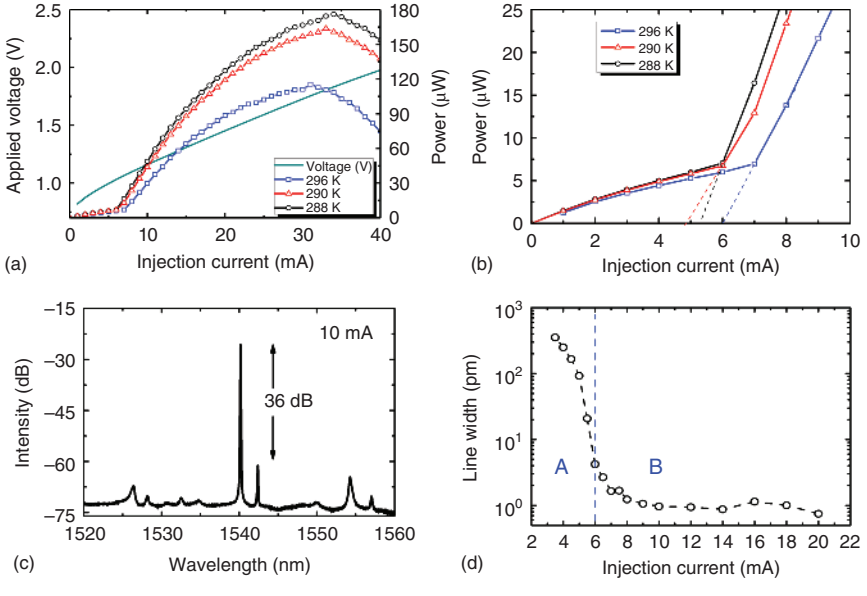

Figure 1.4 (a) Output power coupled into a multiple-mode fiber vs. the injection current, (b) the power vs. the injection current around threshold, (c) lasing spectra at 10 mA, and (d) lasing-mode linewidth vs. injection current, for a microdisk laser connected to a 2-μm-width output waveguide with a radius of 8 μm.

at 1540.3 nm. The FWHM of the lasing mode vs. the injection current at 288 K is shown in Figure 1.4d, where the FWHMs in A and B regions divided by a vertical solid line are directly measured using an optical spectrum analyzer at the finest resolution of 0.02 nm, and estimated from the FWHM of the beating microwave signal by mixing the outputs of the microdisk laser and a tunable laser [32]. The measured FWHM of the beating microwave can be considered as the FWHM of the microdisk laser, as its linewidth is much larger than that of the tunable laser. The FWHMs of the lasing mode are 250, 166, 92.5, 20.8, 4.2, and 1.0 pm at 4, 4.5, 5, 5.5, 6, and 10 mA, respectively, which varies greatly around the threshold. We can estimate mode Q factors of 1.7×10^4, 7.4×10^4, and 3.7×10^5 from the FWHMs at the currents of 5, 5.5, and 6 mA. The mode Q factor of 1.7×10^4 measured at 5 mA, about the intercept of the extrapolated dashed line with the current axis in Figure 1.4b, is in agreement with that obtained by numerical simulation for two-dimensional microcavity under effective index approximation. The agreement indicates that the choice of the intercept current is a better approximation for measuring passive mode Q factor than using the FWHM at the kink position of the power vs. current.

1.5 Book Overview

In this book, we present an overview of the principle, design, and application of semiconductor microlasers, especially for directional emission microlasers based on polygonal optical microcavities. In Chapter 2, we derive an eigenvalue equation for multilayer complex slab optical waveguides, give an optical confinement factor based on the relation between mode gain and material gain, and discuss the effective index method for reducing three-dimensional (3D) waveguide to a two-dimensional (2D) problem. In Chapter 3, we simply introduce finite-difference time-domain method and Padé approximation with Baker's algorithm for simulating optical microcavities, and give some numerical results for simulating mode frequencies and mode Q factors of microcavities and the transmission coefficient for optical microring add-drop filters. Chapter 4 presents an eigenvalue equation for 2D microdisk and deformed and chaotic microcavity lasers for directional emission. In Chapter 5, we summarize unidirectional emission microdisk lasers based on mode coupling due to connection with an output waveguide, and propose to realize unidirectional emission hybrid microlaser on silicon wafer by wafer bonding using locally deformed microring resonator. In Chapter 6, we derive analytical mode solution for equilateral triangle resonator, and compare with numerical simulated results and lasing spectra of fabricated devices. In Chapter 7, we present analytical-mode solution for square microcavities and discuss the formation of high-Q coupled modes. Furthermore, the enhancement of mode Q factors by circular-sided square microcavities is discussed, and dual-mode lasing microlasers are designed and realized in addition to single-mode microlasers. In Chapter 8, we discuss mode characteristics for polygonal microcavities based on group theory especially for hexagonal microcavity, and present lasing characteristics for hexagonal and octagonal and circular-sided hexagonal microlasers. In Chapter 9, we consider the vertical radiation loss for 3D

semiconductor microcavities with vertical semiconductor waveguiding, and discuss lateral size limit for such microcavities due to the vertical radiation loss. In Chapter 10, we summarize nonlinear dynamics for microlasers subject to optical injection and integrated microlasers with mutually optical injection. Finally, in Chapter 11, we demonstrate a hybrid cavity composed of a Fabry–Pérot (FP) cavity and a square microcavity for mode selection. Stable single-mode operation with high coupling efficiency to a single mode fiber is realized, and controllable optical bistability is achieved for all-optical signal processing.

References

1 Chang, R.K. and Campillo, A.J. (eds.) (1996). *Optical Processes in Microcavities*. Singapore: World Scientific.
2 Vahala, K.J. (ed.) (2004). *Optical Microcavities*. Singapore: World Scientific.
3 Cao, H. and Wiersig, J. (2015). Dielectric microcavities: model systems for wave chaos and non-Hermitian physics. *Rev. Mod. Phys.* 87: 61–111.
4 Vahala, K.J. (2003). Optical Microcavities. *Nature* 424: 839–846.
5 Rayleigh, L. (1910). The problem of the whispering gallery. *Philos. Mag.* 20: 1001–1004.
6 Matsko, A.B. and Ilchenko, V.S. (2006). Optical resonators with whispering-gallery modes – part I: basics. *IEEE J. Sel. Top. Quantum Electron.* 12: 3–14.
7 Ward, J. and Benson, O. (2011). WG microresonators: sensing, lasing and fundamental optics with microspheres. *Laser Photonics Rev.* 5: 553–570.
8 He, L.N., Ozdemir, S.K., and Yang, L. (2013). Whispering gallery microcavity lasers. *Laser Photonics Rev.* 7: 60–82.
9 Mccall, S.L., Levi, A.F.J., Slusher, R.E. et al. (1992). Whispering-gallery mode microdisk lasers. *Appl. Phys. Lett.* 60: 289–291.
10 Nockel, J.U. and Stone, A.D. (1997). Ray and wave chaos in asymmetric resonant optical cavities. *Nature* 385: 45–47.
11 Yang, Y.D. and Huang, Y.Z. (2016). Mode characteristics and directional emission for square microcavity lasers. *J. Phys. D: Appl. Phys.* 49: 253001.
12 Ilchenko, V.S. and Matsko, A.B. (2006). Optical resonators with whispering-gallery modes – part II: applications. *IEEE J. Sel. Top. Quantum Electron.* 12: 15–32.
13 Little, B.E., Chu, S.T., Haus, H.A. et al. (1997). Microring resonator channel dropping filters. *J. Lightwave Technol.* 15: 998–1005.
14 Schwelb, O. (2004). Transmission, group delay, and dispersion in single-ring optical resonators and add/drop filters – a tutorial overview. *J. Lightwave Technol.* 22: 1380–1394.
15 Heebner, J., Grover, R., and Ibrahim, T. (2008). *Optical Microresonators: Theory, Fabrication, and Applications*. London: Springer-Verlag.

16 Poon, A.W., Luo, X.S., Xu, F., and Chen, H. (2009). Cascaded microresonator-based matrix switch for silicon on-chip optical interconnection. *Proc. IEEE* 97: 1216–1238.

17 Xu, Q.F., Schmidt, B., Pradhan, S., and Lipson, M. (2005). Micrometre-scale silicon electro-optic modulator. *Nature* 435: 325–327.

18 Vollmer, F. and Arnold, S. (2008). Whispering-gallery-mode biosensing: label-free detection down to single molecules. *Nat. Methods* 5: 591–596.

19 Zhu, J.G., Ozdemir, S.K., Xiao, Y.F. et al. (2010). On-chip single nanoparticle detection and sizing by mode splitting in an ultrahigh-*Q* microresonator. *Nat. Photonics* 4: 46–49.

20 He, L.N., Ozdemir, K., Zhu, J.G. et al. (2011). Detecting single viruses and nanoparticles using whispering gallery microlasers. *Nat. Nanotechnol.* 6: 428–432.

21 Peter, E., Senellart, P., Martrou, D. et al. (2005). Exciton-photon strong-coupling regime for a single quantum dot embedded in a microcavity. *Phys. Rev. Lett.* 95: 067401.

22 Fujita, M., Ushigome, R., and Baba, T. (2000). Continuous wave lasing in GaInAsP microdisk injection laser with threshold current of 40 mu A. *Electron. Lett.* 36: 790–791.

23 Yang, Y.D. and Huang, Y.Z. (2007). Symmetry analysis and numerical simulation of mode characteristics for equilateral-polygonal optical microresonators. *Phys. Rev. A* 76: 023822.

24 Jonaš, A., McGloin, D., and Kiraz, A. (2015). Droplet lasers. *Opt. Photonics News* 26 (5): 36–43.

25 Humar, M. and Yun, S.H. (2015). Intracellular microlasers. *Nat. Photonics* 9: 572–576.

26 Del'Haye, P., Schliesser, A., Arcizet, O. et al. (2007). Optical frequency comb generation from a monolithic microresonator. *Nature* 450: 1214–1217.

27 Lee, H., Chen, T., Li, J. et al. (2012). Chemically etched ultrahigh-*Q* wedge-resonator on a silicon chip. *Nat. Photonics* 6: 369–373.

28 Schawlow, A.L. and Townes, C.H. (1958). Infrared and optical masers. *Phys. Rev.* 112: 1940–1949.

29 Henry, C.H. (1982). Theory of the linewidth of semiconductor-lasers. *IEEE J. Quantum Electron.* 18: 259–264.

30 Bagheri, M., Shih, M.H., Choi, S.J. et al. (2009). Microcavity laser linewidth close to threshold. *IEEE J. Quantum Electron.* 45: 935–939.

31 Coldren, L.A. and Corzine, S.W. (1995). *Diode Lasers and Photonic Integrated Circuits*. New York: Wiley.

32 Zou, L.X., Huang, Y.Z., Liu, B.W. et al. (2015). Nonlinear dynamics for semiconductor microdisk laser subject to optical injection. *IEEE J. Sel. Top. Quantum Electron.* 21 (6): 1800408.